


 Cite this: *RSC Adv.*, 2023, **13**, 12023

## Synthesis and characterization of low surface energy thermoplastic polyurethane elastomers based on polydimethylsiloxane

Jie Sun, Xiaobin Zou, Zhiqian Xu and Zhen Ge\*

Organosilicon modified polyurethane elastomers (Si-MTPUs) were synthesized in order to improve the anti-graffiti property of thermoplastic polyurethane elastomers (TPUs). Si-MTPUs were prepared from polydimethylsiloxane (PDMS) and polytetramethylene glycol (PTMG) as mixed soft segment, 1,4-butanediol (BDO) and imidazole salt ionic liquid *N*-glyceryl-*N*-methyl imidazolium chloride ( $[\text{MIM}_{1,\text{g}}\text{Cl}]$ ) used as chain extender, and 4,4'-dicyclohexylmethane diisocyanate (HMDI). The structure, thermal stability, mechanical properties and physical crosslinking density of Si-MTPUs were characterized by Fourier transform infrared spectroscopy (FTIR), thermogravimetry analysis (TGA), mechanical test and low field nuclear magnetic resonance. Surface energy and water absorption were characterized by static contact angle test and water resistance test, and anti-graffiti and self-cleaning properties were characterized with water, milk, ink, lipstick, oily markers and spray paint. It was found that the mechanical properties of Si-MTPU-10 with the content of PDMS 10 wt% were optimized, with a maximum tensile strength of 32.3 MPa and elongation at break of 656%. Surface energy reached the minimum value of  $23.1 \text{ mN m}^{-1}$  with the best anti-graffiti performance, which no longer decreased with the increase of PDMS contents. This work provides novel idea and strategy for the preparation of low surface energy TPUs.

 Received 20th February 2023  
 Accepted 29th March 2023

 DOI: 10.1039/d3ra01142a  
[rsc.li/rsc-advances](http://rsc.li/rsc-advances)

## 1 Introduction

TPUs are a group of thermoplastic polymers containing a considerable number of urethane segments,<sup>1</sup> with similar mechanical and thermal properties compared to thermosetting rubber and similar processing technique compared to plastic. TPUs have several outstanding properties, such as high elasticity and strength, easy processing, cold resistance and wear resistance, water resistance and oil resistance,<sup>2–4</sup> therefore, TPUs are widely used in aerospace, electronic appliances, medical devices and other fields.<sup>5,6</sup> TPUs, however, are frequently exposed in complex environment such as dust, rain and oil stains in the process of use. It is difficult for TPUs without low surface energy characteristic to remove these adhering pollutants. In the long term, it will not only damage mechanical property, but also reduce service life because of weakening molecular chain force.<sup>7,8</sup>

Molecules on the liquid/solid surface are subjected to unbalanced forces and generate additional energy compared with the internal molecules, which is defined as the surface energy of the liquid/solid.<sup>9</sup> Low surface energy materials are free from contaminants, easy to clean, and have excellent self-lubricating properties and low friction properties.<sup>10</sup> It is

reported that polymers have anti fouling effect when the surface energy is less than  $25 \text{ mJ m}^{-2}$ , which means that the contact angle between polymers and liquid is larger than  $98^\circ$ .<sup>11</sup> The main chain of TPUs contains hydrophilic  $-\text{NH}-\text{COO}-$  groups, which are able to form adhesive film with higher surface free energy. Generally, surface energy of pure TPUs film is above  $40 \text{ mJ m}^{-2}$ ,<sup>12</sup> therefore, TPUs are not stain resistant.

Organosilicon compounds refer to the compounds containing Si–O bonds and at least one organic group is directly connected with silicon atom. The main chain of organosilicon compounds is very flexible, and its intermolecular interaction is far less than that of hydrocarbons.<sup>13</sup> The surface energy, therefore, is much lower than the hydrocarbons with the same molecular weight. Moreover, organosilicon compounds have excellent stain resistance, heat resistance and weather resistance.<sup>14</sup> Introducing silicon compound into TPUs can effectively reduce their surface energy and improve their hydrophobicity.<sup>15,16</sup>

Cui<sup>17</sup> used hydroxyl terminated PDMS and PCL to synthesize TPU to study the effect of PDMS content on the microscopic morphology and hydrophobicity of TPU. The results showed that with the increase of PDMS in TPU, the degree of micro phase separation and hydrophobicity increased; when the contents of PDMS were 32.3 wt%, the static contact angle reached the maximum value of  $117^\circ$ .

Luo<sup>18</sup> prepared the hydroxyl terminated WPU emulsion grafted with PDMS, and then it was cross-linked with

School of Materials Science and Engineering, Beijing Institute of Technology, Beijing, 100081, China. E-mail: [gzandlsy@bit.edu.cn](mailto:gzandlsy@bit.edu.cn)



hexamethoxymethyl melamine (HMMM) to prepare a new antifouling coating. It was reported that this coating remained significant anti-graffiti and self-cleaning properties against oily markers, water, hexadecane, fingerprint liquid, and common liquids in life (milk, coffee, ink and cooking oil). Especially, the coating could maintain excellent anti-graffiti ability even when bent or impacted.

S. Kim<sup>19</sup> synthesized polyurethane zwitterionic sulfobetaine (PDMS-SB-UU) using PDMS as soft segment, which could be used to make or coat blood contacting equipment, such as catheters, artificial lungs or microfluidic equipment. In order to characterize the antifouling property of PDMS-SB-UU, fibrinogen absorption test and platelet deposition test were carried out. The results showed that the amount of fibrinogen attached to the surface of PDMS-SB-UU was  $3.8 \pm 0.2$  ng, much lower than  $8.4 \pm 0.1$  ng in the control group; and obviously, the surface of control group was covered with activated platelets, while the surface of PDMS-SB-UU showed almost no platelets and signs of activation.

However, as PDMS was a non-polar compound, the polarity and compatibility with TPUs were very different, and phase separation was quite easy to occur in TPUs. Therefore, when the contents of PDMS was very high, the phase separation degree increased and the mechanical properties dropped sharply.<sup>17,20</sup> It has been found that the introduction of ionic liquids into polyurethane molecular chains could significantly improve the mechanical strength of polyurethane due to the strong interaction of ionic bonds in ionic liquids.<sup>8,21</sup> In our previous work, WPU with imidazole salt ionic liquid as chain extender was prepared, and the tensile strength was 36 MPa, higher than ordinary WPU without ionic liquid.<sup>22</sup> Consequently,  $[\text{MIM}_{1,g}]\text{Cl}$ , an ionic liquid, could be chosen as the chain extender to enhance mechanical properties of TPUs. Moreover, the strengthening of the force between the molecular chains due to the introduction of ionic liquids can effectively improve the physical crosslinking density, making it difficult for pollutants to invade the Si-MTPUs interior, and effectively improving their graffiti resistance.<sup>18</sup>

In this research, novel anti-graffiti Si-MTPUs were designed and prepared. According to our strategy, non-toxic PDMS was selected as the TPUs soft segment to provide low surface energy characteristics; in addition,  $[\text{MIM}_{1,g}]\text{Cl}$  was selected as chain extender to improve the mechanical properties and anti-graffiti properties of TPUs. Solution method was used to prepare a series of TPUs by changing the proportion between PDMS and PTMG while fixing the content (10 wt%) of  $[\text{MIM}_{1,g}]\text{Cl}$ . PDMS mass content was controlled between 0 and 20%. The structure, mechanical properties, low surface energy properties and anti-graffiti properties of Si-MTPUs with different contents of PDMS were studied by FTIR, TGA, DSC, mechanical test, static contact angle test and anti-graffiti test.

## 2 Experimental section

### 2.1 Materials

PTMG (Mn = 2000, industrial grade, 98 wt% purity) and HMDI (industrial grade, 98 wt% purity) were purchased from Bayer

Corp (Leverkusen, German). PDMS (Mn = 2000, industrial grade, 98 wt%) was purchased from Dongguan Jiatong Plastic Raw Material Business Department (Guangdong, China). BDO (AR, 99.5 wt%), dibutyltin dilaurate (DBTDL, AR, 99 wt% purity) and tetrahydrofuran (THF, AR, 99 wt%) were purchased from China National Pharmaceutical Group Co. Ltd (Beijing, China).  $[\text{MIM}_{1,g}]\text{Cl}$  was synthesized by ultrasound method.

### 2.2 Synthesis of Si-MTPUs

A typical synthesis procedure was as follow: firstly, a certain amount of PTMG and PDMS were put into a 500 mL three-neck flask equipped with a mechanical stirrer. PTMG and PDMS were dried under vacuum at 100 °C for 1 h. Then quantitative HMDI and 0.1 wt% of total reaction system DBTDL were added into the flask and the pre-polymerization proceeded at 80 °C for 2 h. The NCO-terminated prepolymer was got. Then the condenser tube was loaded. A certain amount of  $[\text{MIM}_{1,g}]\text{Cl}$  and 0.3 wt% of total reaction system DBTDL were added and reacted at 110 °C for 5 h. Then the system was cooled down to 55 °C. A certain amount of BDO was added to the reaction system and reacted for 2 h, and THF in moderation was added in time to reduce the viscosity in the process. After the reaction, the product was placed in a tetrafluoroethylene mold, until THF completely volatilized, finally yielding Si-MTPUs. The hard segment content of Si-MTPUs was 50 wt%, and the molar ratio of -NCO/-OH was 1.2. The amounts of raw materials corresponding for different PDMS content were listed in Table 1, and the preparation scheme of Si-MTPUs was presented in Scheme 1.

### 2.3 Characterization

**2.3.1 FTIR.** The FTIR spectra of reactants were obtained by Nicolet 8700 Fourier transform infrared spectrometer (Thermo Fisher Scientific, Waltham, MA, USA). The spectra were collected between  $4000 \text{ cm}^{-1}$  and  $650 \text{ cm}^{-1}$  with a resolution of  $4 \text{ cm}^{-1}$ . Each sample was scanned for 48 times at room temperature.

**2.3.2 Static contact angle.** The contact angles of water, ethylene glycol, glycerine, diiodomethane and formamide on the prepared samples were measured on a OCA20 contact angle goniometer (Germany) by the sessile drop method. 2  $\mu\text{L}$  solvent drops were set onto the surface of Si-MTPUs. After 5 s, the contact angle values of films were got through instrument software analysis. Each sample was measured 3 times, and the average value was taken.

The surface energy of the samples was calculated as:

$$\gamma_s = \gamma_s^{\text{LW}} + 2\sqrt{\gamma_s^- \gamma_s^+} \quad (1)$$

$$\gamma_L = \gamma_L^{\text{LW}} + 2\sqrt{\gamma_L^- \gamma_L^+} \quad (2)$$

$$\begin{aligned} & \left( \gamma_L^{\text{LW}} + 2\sqrt{\gamma_L^+ \gamma_L^-} \right) (1 + \cos \theta) \\ & = 2 \left( \sqrt{\gamma_s^{\text{LW}} \gamma_L^{\text{LW}}} + \sqrt{\gamma_s^+ \gamma_L^-} + \sqrt{\gamma_s^- \gamma_L^+} \right) \end{aligned} \quad (3)$$

where surface energy  $\gamma$  defined as Lifshitz-van der Waals component  $\gamma^{\text{LW}}$  and Lewis acid content  $\gamma^+$ , Lewis alkali content



Table 1 The formula of Si-MTPUs prepared with different content of PDMS

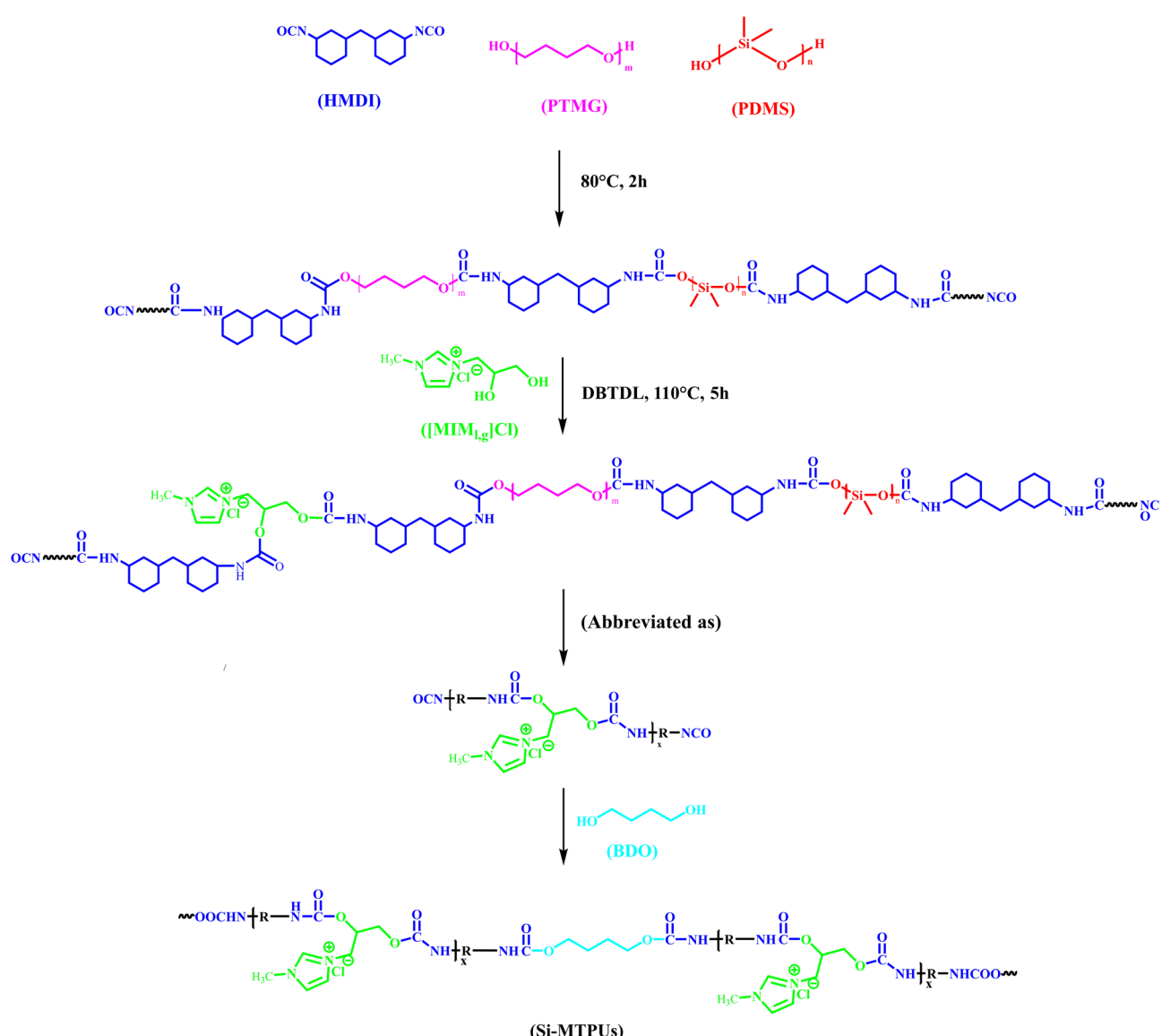
Sample name	<i>m</i> (PTMG) (g)	<i>m</i> (PDMS) (g)	<i>m</i> (HMDI) (g)	<i>m</i> [ $[\text{MIM}_{1,g}\text{Cl}]$ ] (g)	<i>m</i> (BDO) (g)
Si-MTPU-0	25.00	—	18.24	5.00	1.76
Si-MTPU-5	22.50	2.50	18.24	5.00	1.76
Si-MTPU-10	20.00	5.00	18.24	5.00	1.76
Si-MTPU-15	17.50	7.50	18.24	5.00	1.76
Si-MTPU-20	15.00	10.00	18.24	5.00	1.76

$\gamma^-$  form;  $\theta$  was the Young's contact angle. The surface energy parameters of various solvents were shown in Table 2.

**2.3.3 Anti-graffiti test.** In order to investigate the anti-graffiti performance of samples, five different graffiti materials, such as milk tea, coffee, ink, lipstick and green permanent marker were used to imitate the graffiti on the dry paint

samples. In brief, if the graffiti on the surface of Si-MTPUs could be easily wiped away by dry tissues without leaving traces, it meant that the samples had excellent anti-graffiti property.

**2.3.4 Self-cleaning test.** The self-cleaning behavior of Si-MTPUs was tested with muddy water. The samples were placed at the same angle of about  $40^\circ$ , and 2 mL of muddy water

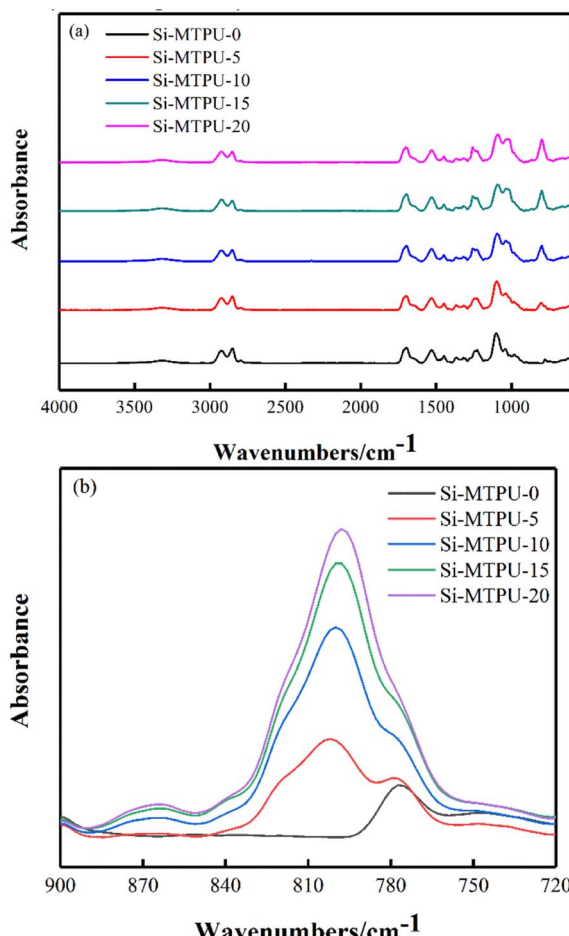


Scheme 1 Preparation of Si-MTPUs.



Table 2 The surface energy parameters of various solvents

Solvents	$\gamma_L$ (mN m <sup>-1</sup> )	$\gamma_L^{LW}$ (mN m <sup>-1</sup> )	$\gamma^+$ (mN m <sup>-1</sup> )	$\gamma^-$ (mN m <sup>-1</sup> )	$\gamma^d$ (mN m <sup>-1</sup> )	$\gamma^p$ (mN m <sup>-1</sup> )
H <sub>2</sub> O	72.8	21.8	25.5	25.5	21.8	51
(CH <sub>2</sub> OH) <sub>3</sub>	64.0	34.0	3.92	57.4	34	30
CH <sub>3</sub> NO	58.0	39.0	2.28	39.6	39	19
CH <sub>2</sub> I <sub>2</sub>	50.8	50.8	0	0	50.8	0
(CH <sub>2</sub> OH) <sub>2</sub>	48.0	29.0	1.92	47.0	33.8	14.2

Fig. 1 FTIR spectrum of Si-MTPUs (a) and FTIR spectrum in the Si-CH<sub>3</sub> stretching region from 700 to 900 cm<sup>-1</sup> (b).

was dropped on the sample surface. The residual stains were recorded with a digital camera.

**2.3.5 Water absorption.** The dry weights of test samples were measured after drying the samples in a vacuum oven at 70 °C for 24 h. Then the samples were immersed into deionized water at room temperature for 24 h. Then after the removal of the excess surface water by filter paper, the weights of samples were measured. And the water absorption was calculated from the following equation:

$$\% \text{ Absorption} = \frac{m - m_0}{m_0} \times 100\% \quad (4)$$

where  $m$  and  $m_0$  were the mass of samples after immersion, and in the dry state, respectively.

**2.3.6 TGA.** TGA studies were performed by a TGA/DSC1 thermogravimetric analyzer (METTLER TOLEDO, Zurich, Switzerland). The sample were scanned at a scanning rate of 10 °C min<sup>-1</sup> from 30 °C to 600 °C under N<sub>2</sub> atmosphere. The specimen of 5–10 mg was taken in alumina crucible and placed in TG apparatus.

**2.3.7 DSC.** DSC of samples were performed by METTLER DSC1 (METTLER TOLEDO, Zurich, Switzerland). The test temperature range was from –100 °C to 100 °C. The sample mass was 5–10 mg, the heating rate was 10 K min<sup>-1</sup>, N<sub>2</sub> was used as protection, and the gas flow rate was 40 mL min<sup>-1</sup>.

### 2.3.8 Tensile property measurement

According to the GB/T 528-2009 standard, the samples were made into a standard dumbbell shape with thickness maintained at 1 mm ± 0.1 mm. The AGS-J electronic universal testing machine (Excellence in Science, Kyoto, Japan) was used to conduct mechanical tests. Each group tested 5 splines to get the mean value, the test temperature was kept at 25 °C, and the tensile rate was 100 mm min<sup>-1</sup>.

**2.3.9 Low field NMR.** The physical crosslinking density of the samples was characterized at 70 °C using the nuclear magnetic resonance crosslinking density analyzer (Suzhou Newman Electronic Technology Co. Ltd., Jiangsu, China). All measurements were the mean values of four runs.

**2.3.10 Anti bacterial.** The bacterial suspension was dropped onto sterilized PU membrane (control) and Si-MTPU-10 membranes (1 × 1 cm<sup>2</sup>) are incubated at 37 °C for 4 h. Then 50 µL of bacterial suspension was dropped onto LB agar plates end evenly coated. After incubation at 37 °C for 24 h, the number of viable bacterial colonies was counted for each membrane. According to the following formula, the antibacterial activity was calculated by the number of colonies of experimental sample (B) and the negative control (A):

$$\text{Antibacterial activity (\%)} = \frac{A_{\text{negative control}} - B_{\text{sample}}}{A_{\text{negative control}}} \quad (5)$$

## 3 Results and discussion

### 3.1 FT-IR

Fig. 1(a) showed the full infrared spectra of Si-MTPUs with different PDMS contents. The absence of the –NCO group



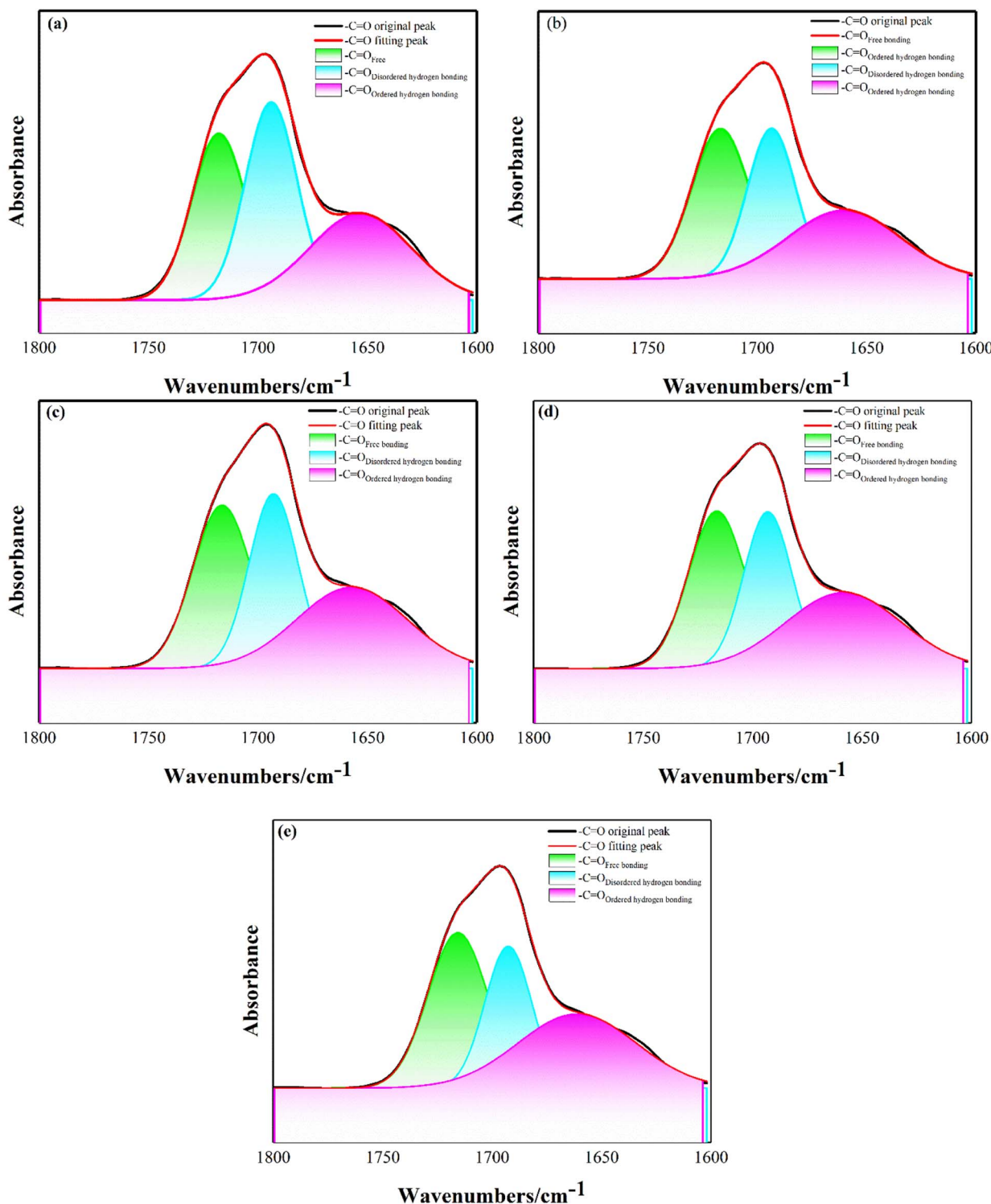


Fig. 2 Fitting peak separation in FTIR spectrum of  $-\text{C=O}$  (a: Si-MTPU-0, b: Si-MTPU-5, c: Si-MTPU-10, d: Si-MTPU-15, e: Si-MTPU-20).

absorption peak at  $2200\text{ cm}^{-1}$  indicated that HMDI has been reacted completely. The absorption peaks at  $3320\text{ cm}^{-1}$  and  $1712\text{ cm}^{-1}$  were corresponded to the formation of urethane ( $-\text{NH}-\text{COO}-$ ) by reaction of  $-\text{OH}$  and  $-\text{NCO}$  group. The peaks at  $2924\text{ cm}^{-1}$  and  $2850\text{ cm}^{-1}$  were attributed to the stretching vibration of  $-\text{CH}_3$  and  $-\text{CH}_2-$  groups. The peaks at  $1537\text{ cm}^{-1}$

were attributed to  $-\text{NH}-$  bending vibration and  $\text{C}-\text{N}$  stretching vibration. The absorption peaks at  $1450\text{ cm}^{-1}$  (stretching vibration peak of  $-\text{C}=\text{C}-$  and  $-\text{C}=\text{N}-$  of imidazole ring),  $1309\text{ cm}^{-1}$  (antisymmetric stretching vibration peak of the imidazole ring) and  $1230\text{ cm}^{-1}$  (the symmetric stretching vibration peak of imidazole ring) demonstrated that  $[\text{MIM}_{1,g}\text{Cl}]$

Table 3 The results of  $-\text{C}=\text{O}$  group hydrogen bonding by fitting the FTIR spectrum

Samples	Si-MTPU-0	Si-MTPU-5	Si-MTPU-10	Si-MTPU-15	Si-MTPU-20
$-\text{C}=\text{O}_{\text{Free bonding}} (\text{cm}^{-1})$	1718	1716	1716	1717	1716
Integral value	4.00	4.76	5.14	4.62	4.93
$-\text{C}=\text{O}_{\text{Disordered hydrogen bonding}} (\text{cm}^{-1})$	1694	1693	1692	1693	1692
Integral value	4.56	4.04	4.55	3.88	3.54
$-\text{C}=\text{O}_{\text{Ordered hydrogen bonding}} (\text{cm}^{-1})$	1653	1658	1657	1660	1657
Integral value	3.90	4.71	4.78	4.12	4.68
HI	2.11	1.83	1.82	1.73	1.67

has been reacted and formed polyurethane chain.<sup>23</sup> The peaks at 1043  $\text{cm}^{-1}$  (stretching vibration of  $-\text{Si}-\text{O}-\text{Si}-$ ) and 804  $\text{cm}^{-1}$  (stretching vibration of  $-\text{C}-\text{Si}-$ ) demonstrated that PDMS has been reacted and formed into polyurethane chain. Moreover, with the increase of PDMS, as shown in Fig. 1(b), the absorption peak intensity of  $-\text{C}-\text{Si}-$  gradually increased.

There were a large number of functional groups which can form hydrogen bonds in polyurethane, such as amino, carbonyl, ether oxygen. Hydrogen bonding was one of the most significant characteristics of polyurethane, which greatly affected the morphology and mechanical properties of PUs.<sup>24-26</sup> As the poor compatibility between PDMS and PTMG, Si-MTPUs would undergo significant micro phase separation, which would change the hydrogen bonding degree of  $-\text{C}=\text{O}$ .<sup>27</sup> Therefore, in order to study the influence of PDMS contents on Si-MTPUs micro phase separation, the linear fitting and Gaussian peak splitting were used to fit the carbonyl FT-IR characteristic absorption peak in this section, as shown in Fig. 2 and Table 3.

It could be seen from Fig. 2 that hydrogen bonding made the absorption peak of  $-\text{C}=\text{O}$  bond into three peak: the  $-\text{C}=\text{O}_{\text{Free}}$  peak around 1715  $\text{cm}^{-1}$ , the  $-\text{C}=\text{O}_{\text{Disordered hydrogen bonding}}$  peak around 1690  $\text{cm}^{-1}$  and the  $-\text{C}=\text{O}_{\text{Ordered hydrogen bonding}}$  peak around 1660  $\text{cm}^{-1}$ .<sup>28</sup> The proportion of hydrogen bonds formed in the  $-\text{C}=\text{O}$  groups could be measured by carbonyl hydrogen bond index (HI), which was calculated with the formula:

$$\text{HI} = \frac{A_{\text{H}}}{A_{\text{F}}} \quad (6)$$

where  $A_{\text{H}}$  was the integral value of hydrogen bonding  $-\text{C}=\text{O}$  peaks (including  $-\text{C}=\text{O}_{\text{Disordered hydrogen bonding}}$  peak and  $-\text{C}=\text{O}_{\text{Ordered hydrogen bonding}}$  peak),  $A_{\text{F}}$  was the integral value of free bonding  $-\text{C}=\text{O}$  peaks. The value depicted in Table 3 showed

that as the contents of PDMS increased, HI value decreased gradually, indicating that the micro phase mixing decreased and micro phase separation was improved. The reason might be that PDMS, which was non-polar and did not contain hydrogen bonding groups, would reduce the compatibility with polyurethane, and extend micro phase separation.<sup>29</sup>

### 3.2 Static contact angle

The static contact angle test could calculate the surface energy and reflect the influence of PDMS on the surface wettability of Si-MTPUs. Table 4 listed the contact angle values and surface energy results of Si-MTPUs corresponding to different PDMS contents. It could be seen from Table 4 that when all the soft segments were PTMG, each contact angle value was the minimum and the surface energy the maximum. As the contents of PDMS increased, the static contact angle of Si-MTPUs increased continuously, like the water contact angle, from 89.4° to 106.8°. And the surface energy values decreased from 36.1  $\text{mN m}^{-1}$  to 23.1  $\text{mN m}^{-1}$ . These results indicated that the introduction of PDMS into TPU chain could effectively reduce surface free energy, as the non-polarity of PDMS would promote the micro phase separation in the microstructure and cause PDMS segment near the surface layer tending to migrate to the surface of Si-MTPUs. When PDMS segments migrated to the surface, the  $-\text{CH}_3$  in PDMS tended to combine with the polarity of polyurethane internally, while the  $\text{Si}-\text{O}$  chains tended to bugle in the air, forming a hydrophobic surface.<sup>30-32</sup> Therefore, when the contents of PDMS reached 10 wt%, as silicon element was enriched to saturated state on polyurethane surface, increasing PDMS contents would not reduce surface energy of Si-MTPUs.

Table 4 Contact angles and surface energies of Si-MTPUs

Samples	Contact angle (°)					Surface energy ( $\text{mN m}^{-1}$ )
	$\text{H}_2\text{O}$	$(\text{CH}_2\text{OH})_2$	$(\text{CH}_2\text{OH})_3$	$\text{CH}_3\text{NO}$	$\text{CH}_2\text{I}_2$	
Si-MTPU-0	89.4	70.9	84.0	42.7	76.6	36.1
Si-MTPU-5	103.2	92.2	103.5	55.8	94.4	25.7
Si-MTPU-10	106.8	91.9	104.4	64.7	93.7	23.1
Si-MTPU-15	104.9	91.7	104.0	65.3	93.6	23.3
Si-MTPU-20	103.5	88.6	101.6	64.9	90.3	23.7



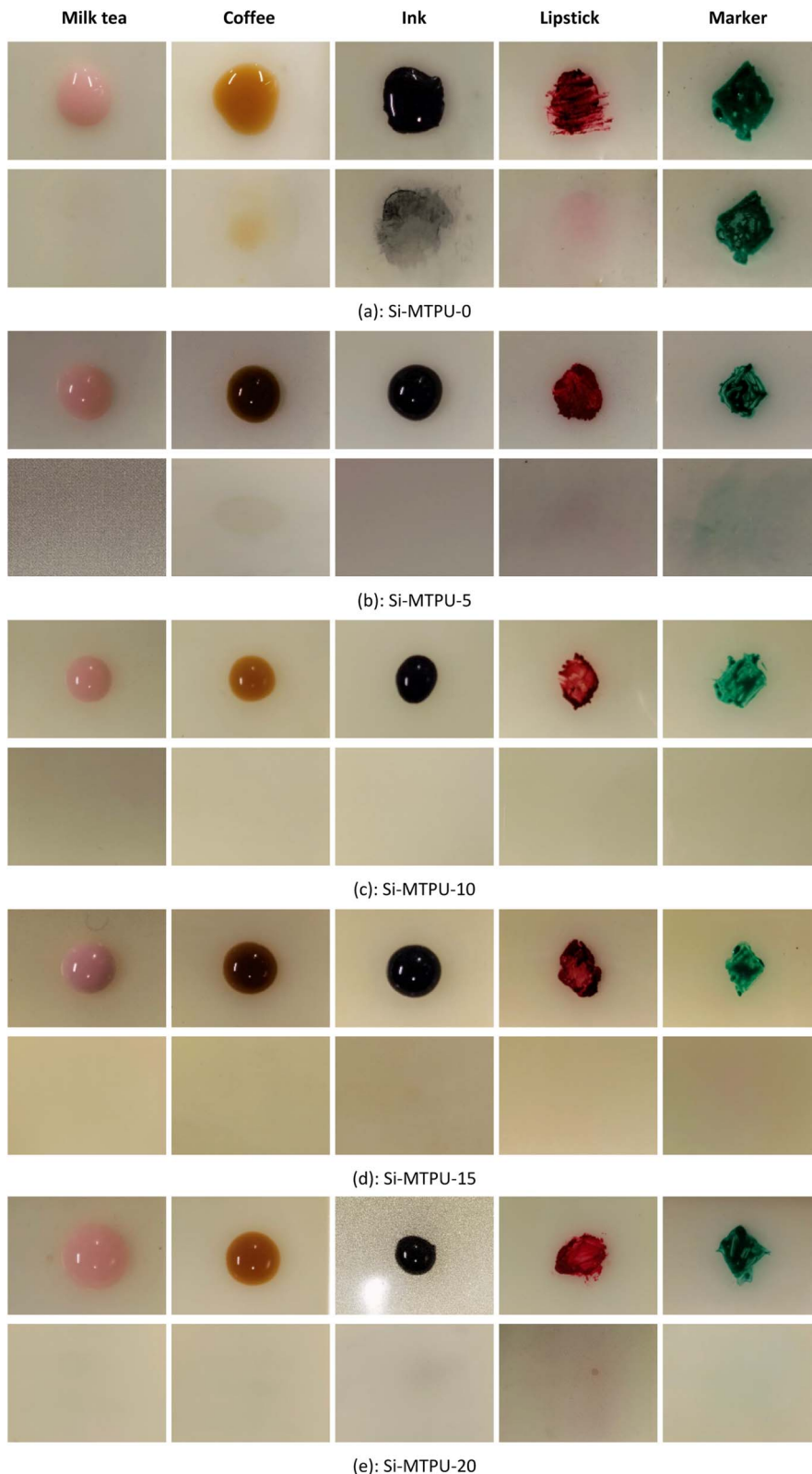


Fig. 3 Surface appearance of Si-MTPUs before and after graffiti removal.

### 3.3 Anti-graffiti analysis

In practical applications, the surface of TPUs was easily contaminated by water and/or oil-based liquid. Therefore, the anti-graffiti

performance of different liquid coatings was tested, as shown in Fig. 3. It could be seen that for Si-MTPU-0, most of the stains were difficult to wipe clean, leaving traces on the surface. Especially the



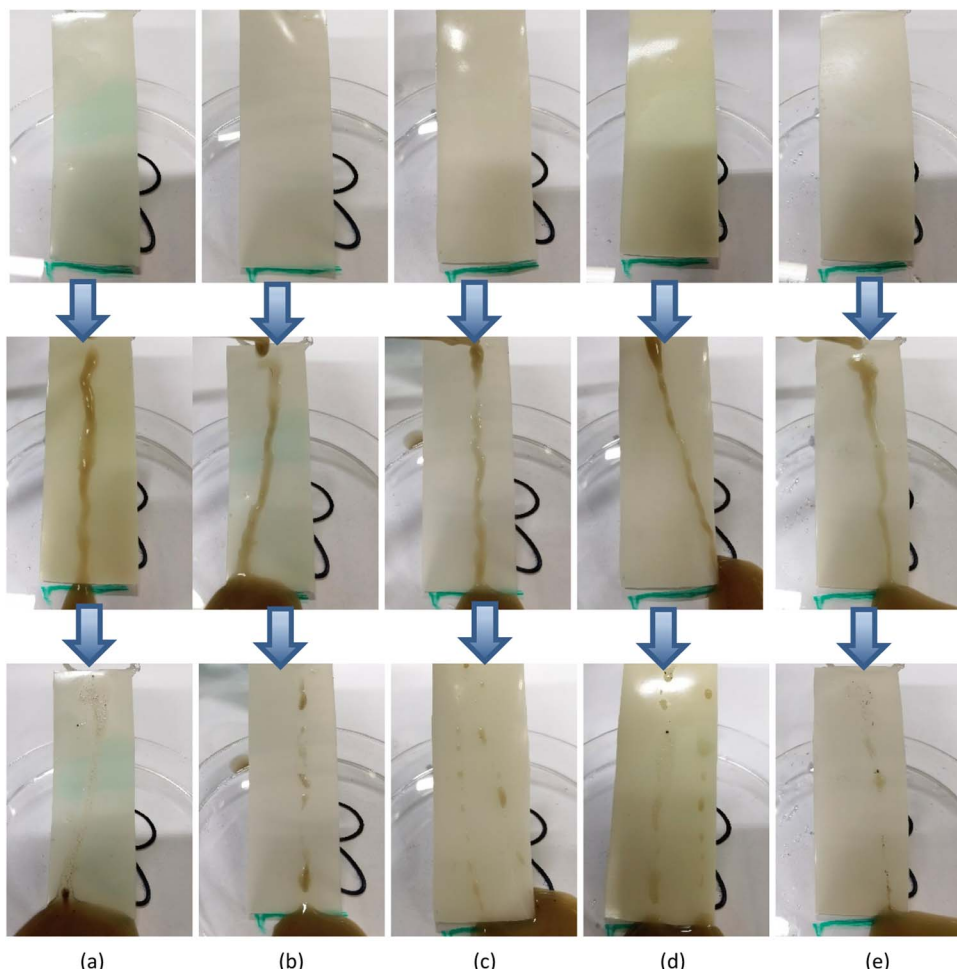


Fig. 4 The phenomenon of self-cleaning test of Si-MTPUs (a: Si-MTPU-0, b: Si-MTPU-5, c: Si-MTPU-10, d: Si-MTPU-15, e: Si-MTPU-20).

ink, containing minerals and carbon, left a lot of black stains after wiping; and the trace of oily marker was hardly erased by dry tissues. When PDMS was introduced into polyurethane chains, all kinds of pollutants on the sample surface could be obviously

removed after wiping, especially when the contents of PDMS reached 10 wt%, indicating that Si-MTPUs achieved superior anti graffiti ability. However, when the PDMS contents was 20 wt%, red and green residues could still be observed on Si-MTPU-20 surface after wiping lipstick and green marker respectively due to physical crosslinking density decreased (as shown in 3.2.9). The excellent anti-graffiti ability of Si-MTPUs was not only related to the low surface energy, but also related to the high crosslinking density. The lower surface energy was, the less likely the pollutants adhered to the surface of Si-MTPUs; and the greater crosslinking density was, the less likely the pollutants penetrated into the interior of Si-MTPUs and the easier to be removed.<sup>33,34</sup>

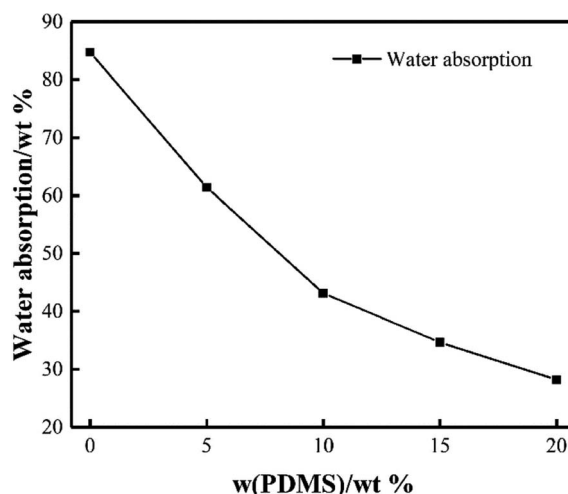


Fig. 5 The water absorption results of Si-MTPUs.

### 3.4 Self-cleaning analysis

Muddy water as a contamination source was mainly used to simulate the natural environment. It could be seen from Fig. 4 that when muddy water was dropped over the Si-MTPUs surface with the similar flow rate, the muddy water mark on Si-MTPU-0 surface was the thickest, which was easier to spread around, and finally stuck to the surface, leaving a pollution mark. As a comparison, the mud flow marks of the other four Si-MTPUs were narrow, with no pollutant diffusion and less mud left on

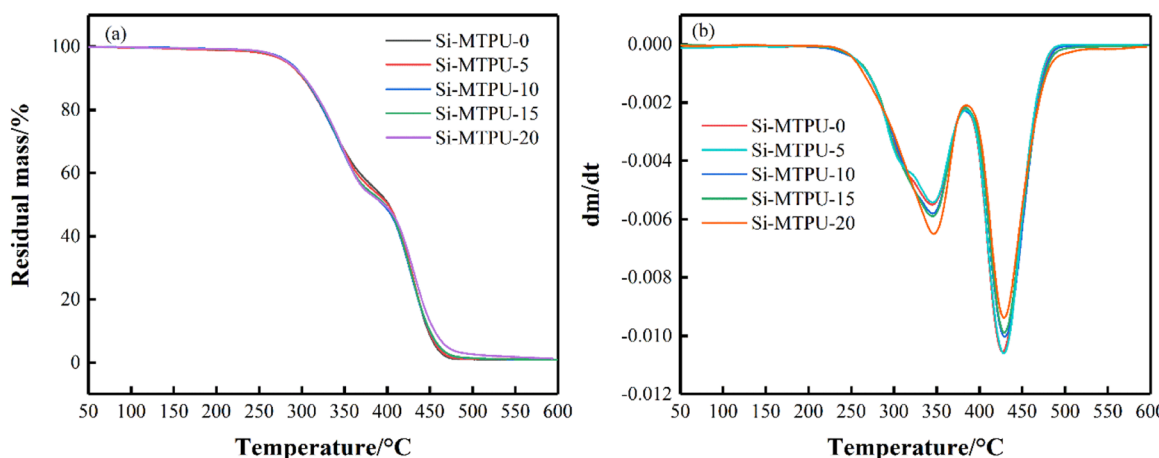


Fig. 6 TGA curves (a) and DTG curves (b) of Si-MTPUs.

Table 5 The TGA characteristics of Si-MTPUs<sup>a</sup>

Samples	$T_i$ (°C)	$T_{max1}$ (°C)	$T_{max2}$ (°C)	Char. Yield at 550 °C (%)
Si-MTPU-0	283.2	344.8	427.0	0.76
Si-MTPU-5	282.5	345.4	428.3	0.84
Si-MTPU-10	285.0	345.3	429.6	0.93
Si-MTPU-15	283.9	345.3	429.1	1.08
Si-MTPU-20	283.8	346.4	428.8	1.54

<sup>a</sup>  $T_i$  was the initial decomposition temperature,  $T_{max1}$  was the maximum decomposition temperature of the hard segments, and  $T_{max2}$  was the maximum decomposition temperature of the soft segments.

the sample surface. This also proved that the Si-MTPUs with PDMS had excellent self-cleaning characteristics.

### 3.5 Water resistance test

Fig. 5 showed the water absorption results of Si-MTPUs. It can be seen that with the increase of PDMS contents, the water

absorption decreased gradually from 84.74% to 28.21%. It could be ascribed that PDMS was a hydrophobic compound. With the increase of PDMS contents, plenty of PDMS was concentrated on the Si-MTPUs surface, preventing water molecules from penetrating into the polyurethane, which improved the water resistance.<sup>16</sup> Moreover, when the contents of PDMS enriched on the sample surface reached to saturation, the decrease of its water absorption became slower.

### 3.6 TGA

Thermal properties of Si-MTPUs were studied using TGA and DSC analyses. Fig. 6(a) and (b) showed TG and derivative thermogravimetric (DTG) curves of Si-MTPUs. Table 5 showed the TG

Table 6  $T_g$  of Si-MTPUs

Samples	$T_{gs}$ (°C)	$T_{gh}$ (°C)	$\Delta T$ (°C)
Si-MTPU-0	-76.4	76.2	152.6
Si-MTPU-5	-78.5	76.5	154.0
Si-MTPU-10	-80.1	77.1	157.2
Si-MTPU-15	-82.6	76.1	158.7
Si-MTPU-20	-83.3	77.4	160.7

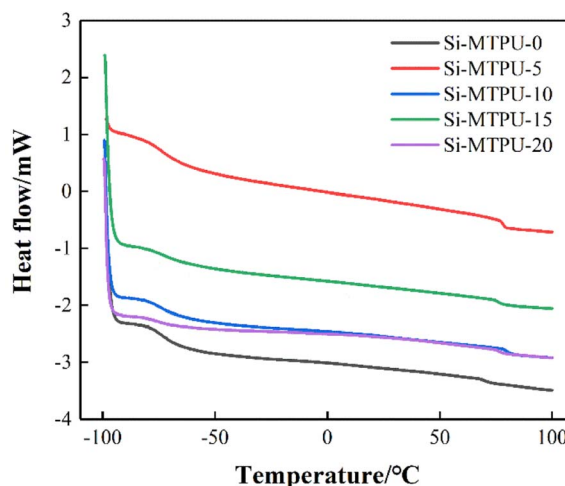


Fig. 7 DSC curves of Si-MTPUs.

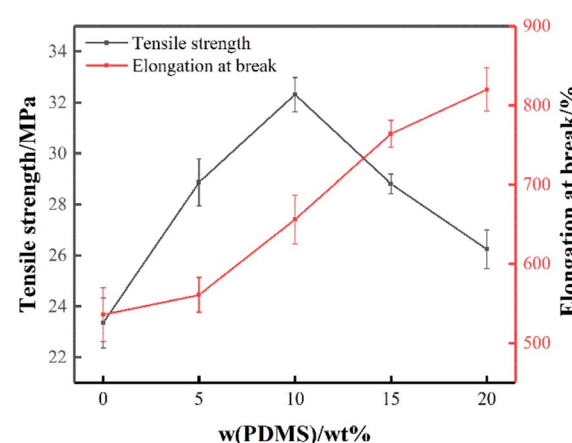


Fig. 8 Mechanical properties of Si-MTPUs.

characteristics of Si-MTPUs. It could be seen that there were two weight loss stages: from 283 °C to 386 °C and from 386 °C to 526 °C, respectively. After 526 °C, the samples were basically decomposed completely. The weight loss of samples below 283 °C was about 5 wt%, which could be caused by the formation of HCl escaped during thermal decomposition of Cl-.<sup>35</sup> Because the thermal stability of the urethane bond in the hard segment was relatively bad, it was generally believed that the thermal weight loss in the first decomposition stage was due to the decomposition of the hard segment, which would be decomposed into isocyanates and polyols. The weight loss rate was 52 wt% average,

which was the same as the hard segment contents of 50 wt% of Si-MTPUs, indicating that the second stage of decomposition would only be started after the basic decomposition of the hard segment was completed. The thermal decomposition of the second stage was related to the thermal decomposition of -C-C-, -C-O- and -Si-O- bond fracture in the soft chain segment, which further decomposed to produce amines, carbon dioxide, hydrocarbons and silicate.<sup>36,37</sup> And it could be seen from Table 5 that with the increase of PDMS, the maximum decomposition temperature of soft segments and the char yield at 550 °C increased gradually, indicating the increasing flame retardancy because of the high bond energy of Si-C bond and the formation of silicon oxide in the residual carbon.<sup>38</sup>

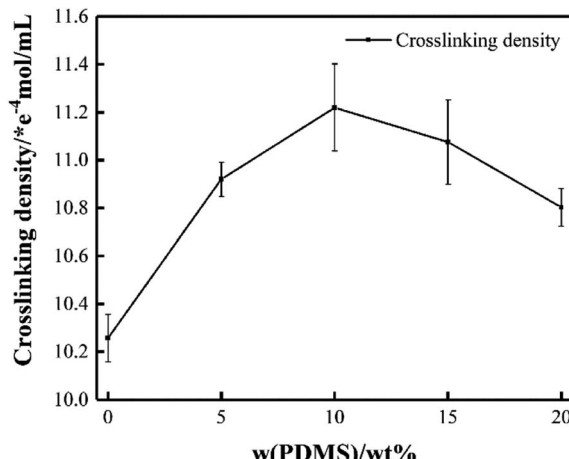


Fig. 9 Cross-linking density values of Si-MTPUs.

### 3.7 DSC

The DSC graphs corresponding to the samples were shown in Fig. 7. It could be seen that there were two thermal transition detected because of the two-phase structure. With the increase of PDMS contents,  $T_g$  of the soft segments decreased gradually, as the molecular chains of PDMS were flexible and the  $T_g$  was lower than PTMG. The difference between the  $T_g$  of soft segments and that of hard segments increased with the increases of PDMS contents, indicating that the phase separation increased, which confirmed the conclusion of fitting peak separation in FTIR spectrum of -C=O (Table 6).<sup>39</sup>

### 3.8 Mechanical test

Fig. 8 illustrated the tensile strength and elongation at break curves of Si-MTPUs with different PDMS contents. It could be

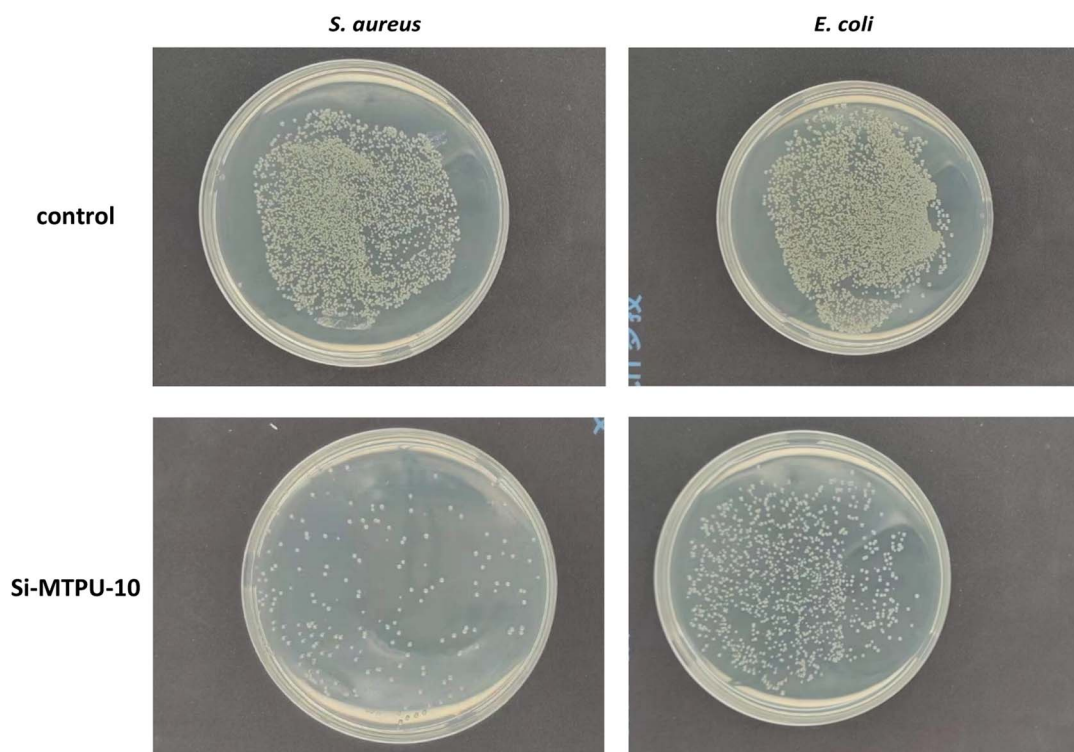


Fig. 10 Antibacterial property of Si-MTPU-10.



seen that with the increase of PDMS contents in Si-MTPUs, the tensile strength increased firstly and then showed a decreasing trend. This can be ascribed that the compatibility between PDMS and polyurethane was poor, and the increase of PDMS contents in the system increased the degree of micro phase separation and enhanced the tensile strength.<sup>40</sup> Therefore, the tensile strength of Si-MTPU-10 was optimized with a maximum value of 32.3 MPa. However, when the contents of PDMS were extremely higher, the weak strength of PDMS reduced the tensile strength, and excessive phase separation reduced the strength.<sup>41</sup> The elongation at break of Si-MTPUs increased from 526% to 797%. The reasons might be that PDMS had great flexibility and the molecular chain was easier to move.<sup>42</sup>

### 3.9 Low field NMR test

Fig. 9 showed the crosslinking density values of Si-MTPUs. It could be seen that with the increase of PDMS contents in samples, the crosslinking density increased firstly and then decreased, consistent with mechanical test results. The reason might be that when the contents of PDMS was lower, because of the poor compatibility between PDMS and PTMG and the low surface energy of PDMS, PDMS chain tended to aggregate on the surface, resulting in a decrease in the number of soft segment molecular chains between hard segments, an increase in crosslinking density.<sup>43</sup> However, when the contents of PDMS was too higher, the interaction of non-polar PDMS molecular chain with amine ester bond and ionic bond in  $[\text{MIM}_{1,g}]Cl$  was reduced, which was shown by the reduction of the number of hard segment micro-regions and the reduction of cross-linking density.

### 3.10 Antibacterial test

With the abuse of antibiotics, more and more bacteria had emerged drug resistance, and even evolved into "superbugs". Therefore, people has been committed to using antibacterial polyurethane materials to replace traditional antibiotics to achieve sterilization effect. Imidazole salts had excellent antibacterial properties.<sup>44</sup> Cations of imidazole salts were absorbed on the bacterial cell wall through electrostatic action, and long alkyl chains of side groups can penetrate into bacteria through the cell membrane, leading to leakage of substances inside cells and death of bacteria.<sup>45</sup> Therefore, antibacterial property was endowed to Si-MTPUs due to the introduction of  $[\text{MIM}_{1,g}]Cl$ . We chose Si-MTPU-10 (because the contents of  $[\text{MIM}_{1,g}]Cl$  in all Si-MTPUs was 10 wt%) for antibacterial activity test. The results were shown in Fig. 10. It could be seen that compared with the control group, the number of plaques in the sample group was significantly reduced, confirming that Si-MTPU-10 had significant antibacterial properties. Moreover, in the sample group, the number of *S. aureus* plaque was significantly higher than that of *E. coli* plaque. The reason might be that *E. coli* was Gram-negative bacterium with stronger electronegativity of cell membrane at physiological pH, which was easier to bind to imidazolium cation, so that the alkyl chain penetrated into the bacterial interior through the cell membrane to inactivate the bacteria. On the other hand, in terms of the cell structure of

bacteria, the cell wall of *S. aureus* contained 15–50 layers of peptidoglycan, while *E. coli* contained only 2–3 layers of peptidoglycan, so *E. coli* was more likely to be killed and inactivated.<sup>46,47</sup>

## 4 Conclusions

In this paper, low surface energy polyurethane elastomers (Si-MTPUs) were prepared using PTMG, PDMS, HMDI,  $[\text{MIM}_{1,g}]Cl$  and BDO. The influence of PDMS contents on Si-MTPUs was mainly studied. The structure of Si-MTPUs was characterized by FTIR firstly. With the increase of PDMS contents in Si-MTPUs, the hydrogen bonding degree of  $-\text{C}=\text{O}$  decreased, the static contact angle gradually decreased to almost constant, anti graffiti property and self-cleaning property improved, the water absorption rate decreased, the maximum decomposition temperature of soft segments increased, tensile strength and crosslinking density increased firstly and then showed decreasing trend. And when the PDMS contents were 10 wt%, the surface energy reached the minimum value of  $23.1 \text{ mN m}^{-1}$ , the tensile strength reached the maximum value of 32.3 MPa, and the crosslink density reached the maximum value of  $11.2 \times 10^{-4} \text{ mol mL}^{-1}$ . Si-MTPUs are promising to be applied to medical device packaging, car cover and anti-graffiti coatings.

## Conflicts of interest

There are no conflicts to declare.

## Notes and references

- M. Khalifa, S. Anandhan, G. Wuzella, H. Lammer and A. R. Mahendran, *Polym.-Plast. Technol. Mater.*, 2020, **59**, 1751–1769.
- A. Atiqah, M. T. Mastura, B. A. A. Ali, M. Jawaid and S. M. Sapuan, *Curr. Org. Synth.*, 2017, **14**, 233–248.
- B. X. Cheng, W. C. Gao, X. M. Ren, X. Y. Ouyang, Y. Zhao, H. Zhao, W. Wu, C. X. Huang, Y. Liu, X. Y. Liu, H. N. Li and R. K. Y. Li, *Polym. Test.*, 2022, **107**, 107489.
- J. Xu, X. Y. Wang, H. W. Ruan, X. R. Zhang, Y. M. Zhang, Z. H. Yang, Q. H. Wang and T. M. Wang, *Polym. Chem.*, 2022, **13**, 2420–2441.
- S. Q. Tian, *Polymers*, 2020, **12**, 1996.
- X. R. Li, J. Li, J. Y. Wang, J. Yuan, F. Jiang, X. Y. Yu and F. P. Xiao, *Constr. Build. Mater.*, 2021, **304**, 1–25.
- D. A. Erofeev, L. N. Mashlyakovskii, E. V. Khomko and G. E. Litosov, *Russ. J. Appl. Chem.*, 2021, **94**, 647–655.
- Y. Xia, N. Zhu, Y. Zhao, J. H. Zhu, H. J. Chen, L. Y. Xu and L. R. Yao, *Materials*, 2023, **16**, 52.
- J. Leitner, P. Slepicka and D. Sedmidubsky, *Chem. Listy*, 2021, **115**, 13–19.
- H. R. Pakravan and F. Memariyan, *Polym.-Plast. Technol. Eng.*, 2017, **56**, 227–239.
- H. Zhao, W. C. Gao, Q. Li, M. R. Khan, G. H. Hu, Y. Liu, W. Wu, C. X. Huang and R. Li, *Adv. Colloid Interface Sci.*, 2022, **303**, 102644.
- P. Krol and B. Krol, *Colloid Polym. Sci.*, 2012, **290**, 879–893.



13 M. K. Raj and S. Chakraborty, *J. Appl. Polym. Sci.*, 2020, **137**, 48958.

14 D. P. Qi, K. Y. Zhang, G. W. Tian, B. Jiang and Y. D. Huang, *Adv. Mater.*, 2021, **33**, 2003155.

15 Z. Luo, Q. Zhang, X. Zhan and F. Chen, *J. Zhejiang Univ., Eng. Sci.*, 2011, **45**, 566–570.

16 X. Ji, H. Z. Wang, X. L. Ma, C. Y. Hou and G. Z. Ma, *RSC Adv.*, 2017, **7**, 34086–34095.

17 Y. Y. Cui, H. W. Pan, J. P. Zhang, L. Cao and C. Z. Zong, *J. Polym. Res.*, 2022, **29**, 218.

18 H. H. Luo, H. Wei, L. Wang, Q. Gao, Y. Chen, J. Xiang and H. J. Fan, *J. Colloid Interface Sci.*, 2022, **628**, 1070–1081.

19 S. Kim, S. H. Ye, A. Adamo, R. A. Orizondo, J. Jo, S. K. Cho and W. R. Wagner, *J. Mater. Chem. B*, 2020, **8**, 8305–8314.

20 B. Chan, S. S. Liow and J. L. Xian, *RSC Adv.*, 2016, **6**, 34946–34954.

21 Y. Q. Dong, H. B. Guo, Z. X. Su, W. J. Wei and X. Q. Wu, *Chem. Eng. Process.: Process Intensif.*, 2015, **89**, 62–69.

22 X. Liu, Y. Zhan, C. Zhao, Y. Su, Z. Ge and Y. Luo, *Polymers*, 2020, **12**, 1513.

23 Y. F. Zhang, J. Z. Liu, J. Li, C. Y. Wang and Q. Ren, *Polym. Bull.*, 2022, **79**, 10295–10311.

24 C. Yu, Y. Cui, H. Fu, L. Mao and L. Zhang, *J. Beijing Univ. Chem. Technol., Nat. Sci. Ed.*, 2012, **39**, 52–57.

25 Y. He, D. L. Xie and X. Y. Zhang, *J. Mater. Sci.*, 2014, **49**, 7339–7352.

26 K. A. Houton and A. J. Wilson, *Polym. Int.*, 2015, **64**, 165–173.

27 S. L. Luo, C. D. Liu, G. F. Gong, H. P. Lai and W. Z. Kong, *Synthesis and Characterization of Polyorganosiloxane Modified Waterborne Polyurethane*, Peoples R China, 2009.

28 A. Niemczyk, A. Piega, A. S. Olalla and M. El Fray, *Eur. Polym. J.*, 2017, **93**, 182–191.

29 H. Fang and L. Wu, *Paint Coat. Ind.*, 2008, **38**, 60–63.

30 B. Han, P. Wang, H. Jin, Z. Hou and X. Bai, *Phys. Lett. A*, 2020, **384**, 126628.

31 J. Chungprempree, J. Preechawong and M. Nithitanakul, *Polymers*, 2022, **14**, 4252.

32 S. H. Zeng, Q. M. Wang, P. P. Chen, Y. Xu, W. Y. Nie and Y. F. Zhou, *Prog. Org. Coat.*, 2022, **165**, 106729.

33 C. Zheng, G. Liu and H. Hu, *ACS Appl. Mater. Interfaces*, 2017, **9**, 25623–25630.

34 X. M. Zhong, H. F. Hu, L. Yang, J. Sheng and H. Q. Fu, *ACS Appl. Mater. Interfaces*, 2019, **11**, 14305–14312.

35 G. Li, E. Li, C. Wang and Y. Niu, *J. Compos. Mater.*, 2015, **49**, 1929–1936.

36 S. Li, Z. Jiang and K. Yuan, *Polym.-Plast. Technol. Eng.*, 2006, **45**, 95–108.

37 Y. Chen, H. He and Z. Liu, *Prog. React. Kinet. Mech.*, 2021, **46**, 1–18.

38 Q. L. Li, S. Q. Song, H. W. Yang, J. C. Wang, J. H. Xiao and Y. Zhang, *Compos. Sci. Technol.*, 2022, **230**, 109758.

39 K. Madhavan and B. S. R. Reddy, *J. Membr. Sci.*, 2006, **283**, 357–365.

40 J. P. Zong, Q. S. Zhang, H. F. Sun, Y. T. Yu, S. J. Wang and Y. H. Liu, *Polym. Bull.*, 2010, **65**, 477–493.

41 M. G. Kim, K. I. Jo, E. Kim, J. H. Park, J. W. Ko and J. H. Lee, *Polymers*, 2021, **13**, 4823.

42 T. C. Liu, M. He, S. J. Feng, Y. M. Liu, X. Zhang, Y. J. Wang, C. F. Mao, X. H. Bu and Y. M. Zhou, *Prog. Org. Coat.*, 2023, **174**, 107315.

43 G. Zheng, M. Lu and X. Rui, *Appl. Surf. Sci.*, 2016, **399**, 272–281.

44 G. S. Andrei, B. F. Andrei and P. R. Roxana, *Mini-Rev. Med. Chem.*, 2021, **21**, 1380–1392.

45 R. Rossi and M. Ciofalo, *Molecules*, 2020, **25**, 5133.

46 Y. F. Yang, H. Q. Hu, Y. Li, L. S. Wan and Z. K. Xu, *J. Membr. Sci.*, 2011, **376**, 132–141.

47 M. Davoudabadi, S. Fahimirad, A. Ganji and H. Abtahi, *J. Biomater. Sci., Polym. Ed.*, 2023, 1–26, DOI: [10.1080/09205063.2023.2170138](https://doi.org/10.1080/09205063.2023.2170138).

